Hindawi
Advances in Materials Science and Engineering
Volume 2020, Article ID 7265941, 14 pages
https://doi.org/10.1155/2020/7265941

Research Article

Study of the Effect of Process Parameters on Surface Profile Accuracy in Single-Point Incremental Sheet Forming of AA1050-H14 Aluminum Alloy

Abdulmajeed Dabwan,[1] **Adham E. Ragab**,[1] **Mohamed A. Saleh**,[2] **Saqib Anwar**,[1] **Atef M. Ghaleb**,[1] **and Ateekh Ur Rehman**[1]

[1]*King Saud University, Department of Industrial Engineering, College of Engineering, Riyadh 11421, Saudi Arabia*
[2]*Private Consultants, Cairo, Egypt*

Correspondence should be addressed to Abdulmajeed Dabwan; abmj999@yahoo.com

Received 30 September 2019; Revised 21 November 2019; Accepted 3 December 2019; Published 8 January 2020

Academic Editor: Tomasz Trzepieciński

Single-point incremental forming is an innovative flexible and inexpensive technique to form sheet products when prototypes or small batches are required. The process allows complex geometries to be produced using a computer numerical control machine, eliminating the need for a special die. This study reports on the effects of four important single-point incremental forming process parameters on produced surface profile accuracies. The profile accuracy was estimated by measuring the side angle errors and surface roughness and also waviness and circularity of the product inner surface. Full factorial design of experiments was used to plan the study, and the analysis of variance was used to analyze and interpret the results. The results indicate that the tool diameter (d), step depth (s), and sheet thickness (t) have significant effects on the produced profile accuracy, while the feed rate (f) is not significant. As a general rule, thin sheets with greater tool diameters yielded the best surface quality. The results also show that controlling all surface quality features is complex because of the contradicting effects of, and interactions between, a number of the process parameters.

1. Introduction

Incremental sheet forming (ISF) is a newly developed technique for the manufacturing thin-sheet metal components, in which a computer numerical control (CNC) machine is used to produce an unlimited variety of geometries by means of a simple generic tool. It offers a number of advantages compared to traditional sheet metal processes, including greater formability limits, lower initial costs, shorter lead-times, and greater process flexibility [1]. The process is suitable for producing prototypes and small batch production in a number of fields, including the automotive industry, the aerospace industry [2], housing, medical implants [3], thin shell dies, and biomedical components [4].

In the ISF process, a simple-shaped forming tool is attached to a general-purpose CNC milling machine, and as the machine table moves according to a preloaded code, the tool applies a preprogrammed deforming load to a sheet metal workpiece clamped to the machine table. The applied load deforms the sheet incrementally into a predefined shape. The ISF processes can be categorized into two primary types: single-point incremental forming (SPIF) and two-point incremental forming (TPIF). The difference between the types is the use of a supporting die underneath the workpiece in TPIF [5].

Iseki and Kumon [6] were the first to develop an incremental forming process. Iseki et al. [7] developed the SPIF process by deforming sheet metal along a path of contour lines using a ball-nosed tool. A number of studies have been conducted on SPIF to investigate the influence of process parameters on geometric accuracy [8] and surface quality [9]. In addition, studies have been presented on the different phenomena observed during the SPIF process such as forming force, material springback, and mechanics of deformation.

Low geometric accuracy is considered to be one of the limitations of the SPIF technique and frequently results in the produced parts deviating significantly from the specified tolerances [10]. A number of studies were conducted aiming at overcoming this problem. Ambrogio et al. [8] studied the dimensional accuracy of the process using numerical and experimental techniques to investigate the geometrical error, that is defined as the difference between the obtained and the desired shapes. The obtained parts were tested using reverse engineering, and the measured geometry was numerically compared with the designed one to quantify the geometrical differences; the result was that thicker sheets and smaller depth steps produced parts of higher quality. Attanasio et al. [5] evaluated the surface quality of the produced parts in two-point incremental forming with full die producing simple pockets. The surface quality was estimated by measuring the waviness of the pocket bottom surface using a coordinate measuring machine (CMM). It was concluded that decreasing both the step depth and scallop height improved the dimensional accuracy, surface quality, and thinning of the part.

Other researchers proposed solutions such as multistage SPIF [11] and an algorithm for correcting the tool path during operation [12]. These solutions required longer production times but resulted in an improved dimensional accuracy. Hussain et al. [13] investigated the effects of five process parameters, namely, sheet thickness (t), step size (s), wall angle, sheet prestraining, and tool radius, on the profile accuracy of the formed parts using response surface techniques. The results indicated that s, wall angle, t, and the interaction between the wall angle and t had significant effects on the profile accuracy of the parts. Ambrogio et al. [14] studied the effects of five parameters, namely, wall angle, t, s, tool radius, and part depth, on the accuracy of the formed parts. The results, using a statistical approach, indicated a satisfactory prediction of the material springback. Because of the problem complexity and the number of considered parameters, a response surface statistical model was implemented. Two satisfactory equations were derived that were able to describe the sheet behavior with respect to the chosen output variables (geometrical error).

Regarding the slope angle, the maximum wall angle is approximately 60–70° for blank thicknesses ranging from 0.8 to 1.5 mm for different series of aluminum alloys [2, 15]. Petek et al. [16] reported the experimental equipment and design of the system for deformation and forming force measurement during SPIF and conducted experiments with wall angles of 40°, 50°, 55°, 60°, 65°, 70°, and 71°. It was determined that the maximum attainable wall angle in forming a cone-shaped part, prior to crack occurrence, was 70°. The material used was 1-mm thick DC05 steel.

Surface roughness resulting from SPIF was also studied by a number of researchers. Hagan and Jeswiet [17] adopted white interferometry scanning to characterize the surface roughness under different spindle speeds and depth increments. The results indicated an exponential increase in the maximum peak-to-valley height as the depth increment size decreased, and little correlation was observed between the roughness and spindle speed. Hussain et al. [18] found that the product surface quality was directly affected by both the lubricant and the lubrication method, although the application of lubricant could be potentially environmentally unfriendly and not cost-effective. Durante et al. [19] proposed an analytical model to calculate the relationship between the surface roughness and ISF parameters, including vertical step depth, wall angle, and tool radius of the forming parts, with a mathematical method that did not take the material properties and deformation of the sheet metal into consideration. They determined that the surface roughness varied with the wall angle, s, and the tool diameter (d), and validated the models by creating pyramidal components with AA7075-T0 sheets.

Liu et al. [20] proposed a methodology to describe a relationship between four process parameters in aluminum parts (feed rate (f), t, d, and s) and overall surface roughness obtained. The results indicated that s and the t are the most significant parameters. Bagudanch et al. [21] concluded that the spindle speed and s are the most critical parameters, and the interactions between f and s, t and d, and spindle speed with f also have a significant influence on the surface roughness. Mugendiran et al. [22] studied incremental forming to optimize surface roughness by controlling the effects of forming parameters. The obtained results indicated that the primary parameters influencing the arithmetic mean surface roughness value (Ra) are f, spindle speed, and t, excluding the interactions among the three parameters. Bhattacharya et al. [23] studied the effect of process parameters on surface roughness by forming pyramidal frustums and truncated conical forms and developed empirical equations for surface finish. Lu et al. [24] improved the surface quality of the final part by developing feature-based tool path generation strategies. Kim and Park [25] improved the surface finish of the sheet during the SPIF process by using a roller-ball tool. Lu et al. [26] developed an oblique roller-ball (ORB) tool to study the effects of friction on surface finish. The results indicated that improved surface quality could be achieved by reducing the friction resistance using the ORB tool.

Formability limit in ISF was the subject of several studies recently. Some researchers built traditional Forming Limit Diagrams (FLDs) to define the formability limit in ISF process [27]. These efforts were criticized by other researchers due to the existence of bending and through thickness sheer in ISF process which limit the use of traditional FLDs [28]. Other researchers focused on the fracture as the criterion for ISF process formability limit, for example, using the maximum formable angle [29] or the maximum formable depth [28] before fracture as the forming limit.

While higher formability can be achieved using ISF than traditional forming techniques, process parameters affect this advantage. Jeswiet et al. [2] studied the effect of some process parameters on the formability of AA 1100 aluminum alloy. His results showed that the formability increases with higher feed rate, smaller tool size, higher sheet thickness, and smaller step size. Ambrogio et al. [1] proved the same results regarding the effect of tool diameter. Same results were obtained by Malhotra et al. [28] relating the tool size and step size to forming limit defined by fracture depth.

Limited studies regarding the development of analytical and empirical models for the evaluation of surface profile quality are available in the literature. This study focuses on the circularity, surface waviness of the side walls, and side wall angle of the parts produced using SPIF. To the best of the knowledge of the authors, no studies investigating the effect of the process parameters on the side surface waviness in SPIF have been reported, and no research has been reported to evaluate the circularity of SPIF-produced parts. The aim of this study is to investigate the process parameters affecting the profile errors and surface roughness in SPIF. Full factorial design is used to design the experimental work using four process parameters: d, f, s, and t. Analysis of variance, regression, and optimization techniques are used to analyze the results.

2. Experiments

Figure 1(a) shows the experimental setup on a CNC milling machine. A dedicated fixture was designed and built to control the relative position between the forming tool and the workpiece. The fixture comprised three separate parts to allow free deformation of the workpiece under the applied load. The initial shape of the workpiece was a square sheet with 240-mm sides, while the deformed area was 200×200 mm.

The selected geometry was a truncated cone-shape with a base diameter of 100 mm and height of 50 mm. The studied process parameters (d, f, s, and t) are shown in Figure 1(b). The spiral tool path was generated using MASTERCAM software to perform the forming of the sheet. Tool contours were created and connected using a transition step method [2].

Forming tools were manufactured from D2 (high-carbon, high-chromium cold-work tool steel) hardened to 63 HRC. The tool shape was cylindrical with a hemispherical tip. To reduce friction between the tool and the workpiece, the tool tip was polished. Two different diameters were used to investigate the effect of d on process output, 10 mm and 20 mm, as shown in Figure 1(c). The machine spindle speed was set to zero rpm, and the tool was inserted into a live center, as shown in Figure 1(a), to allow free rotation with respect to the machine axis in order to reduce friction. This is due to the fact that using the spindle speed cause excessive tearing of the aluminum sheets because of its low strength and low temperature resistance. Furthermore, previous researcher working with aluminum 1050 alloy also employed zero spindle speed that let the tool to rotate freely by live center [30, 31]. Lubricating oil was also used to reduce friction. Figure 1(d) shows one of the produced parts. Forming force was measured using a KISTLER 2825A1 force dynamometer connected to a KISTLER 5019B three-channel charge amplifier. The force components were measured in three directions (x, y, and z) by the load cell. Additionally, the measuring system included charge amplifiers and data acquisition cards to record the measured forces on a PC. The sampling rate of force measurement was 50 Hz.

2.1. Design of Experiment. To estimate the influence of the processing parameters on surface profile accuracy, a full factorial design of experiment (DOE) with four factors and two levels for each factor (16 combinations) was used with three replicates. The four process parameters under consideration were d, f, s, and t.

Table 1 presents the minimum and maximum values of the investigated parameters. These levels were chosen based on the literature and preliminary experiments.

2.2. Geometrical and Dimensional Accuracy Measurement. A Zeiss ACCURA CMM was used to estimate the waviness, circularity, and wall side angle errors of the formed parts. Coordinates of greater than 200 points on each produced part were recorded with an accuracy of 2 μm using a 3 mm diameter CMM probe that was sufficiently small to map the surface features of the produced parts and large enough to avoid the effects of expected nonuniformities due to surface roughness.

The circularity errors were estimated at three locations along the depth of the formed part. The coordinates of 30 points along the circular path in the XY-plane were measured using the CMM, while a constant probe height in the Z direction was maintained. This process was repeated at locations C1, C2, and C3 as shown in Figure 2(a). Figure 2(b) shows a plot of the expected circular hysteresis of a typical circularity test. At each measuring location (C1, C2, and C3), a circle was fitted using the least squares method, and the maximum radial deviations (inside and outside the fitted circle) were detected and recorded (B1 and B2 in Figure 2(b)). The circular deviation was calculated as the maximum radial separation of two concentric circles enveloping the actual path (maximum zone circles) as specified by ISO 230 4:2005(E) [32]. The circularity error was estimated as the summation of the two deviations, B1 + B2.

To estimate the waviness error, the coordinates of approximately 200 inner surface points were selected along four paths (W1, W2, W3, and W4) as shown in Figure 3(a). The four paths were 90° apart, and a line was fitted through the recorded points using the least squares method along each path. The maximum deviations (A1 and A2) from the line were calculated as shown in Figure 3(b). The waviness deviation for each path was estimated as the sum of A1 and A2, as defined by ASME B46.1-1985. The waviness error was calculated as the average of the four deviations of each part.

The side angle is the slope that the side walls of parts make with the horizontal XY-plane, as shown in Figure 1(b). The side angle error was calculated as the absolute value of the difference between the actual and designed side angle (60°). Figure 4(a) shows the setup for the coordinates measuring process using the CMM.

2.3. Surface Roughness Measurement. Surface roughness is a critical parameter that is related to the surface quality of industrial products. Apart from its relationship with the correct functioning of the product, it has a significant impact

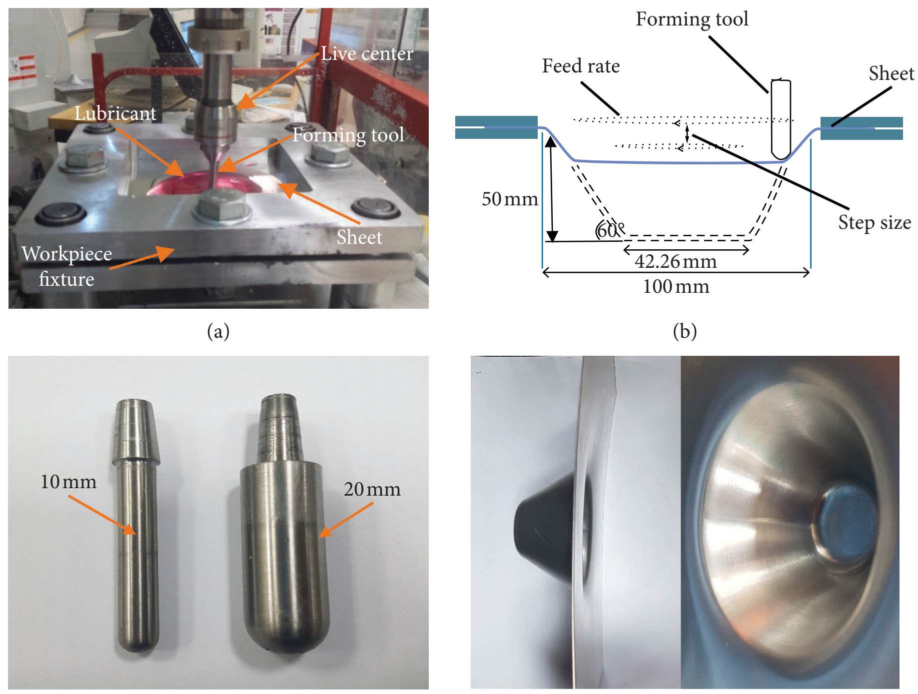

(c) (d)

Figure 1: (a) Experimental setup, (b) part dimensions with the studied process parameters, (c) forming tools, and (d) produced part.

Table 1: Forming parameters and their levels.

Annotation	Experimental parameter	High level	Low level
(d)	Tool diameter (mm)	20	10
(f)	Feed rate (mm/min)	1000	500
(s)	Step size (mm)	1	0.5
(t)	Sheet thickness (mm)	2	1

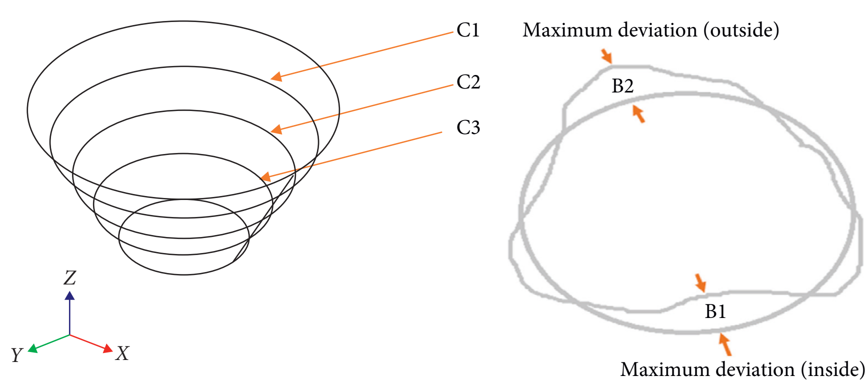

(a) (b)

Figure 2: Circularity path. (a) Level of circular path in XY-plane and (b) circular hysteresis.

on the aesthetics of the final product. The Ra and the maximum height of the profile (Rt) were measured for all produced parts. The roughness was measured using the setup shown in Figure 4(b). The four sides were measured in the part, and each measurement was repeated twice to increase the accuracy. The average values of Ra and Rt were reported as the surface roughness values. For all the measurements, the cutoff length was taken as 0.8 mm and the evaluation length was taken as 4 mm.

3. Results and Discussion

Table 2 presents the DOE matrix and the corresponding results.

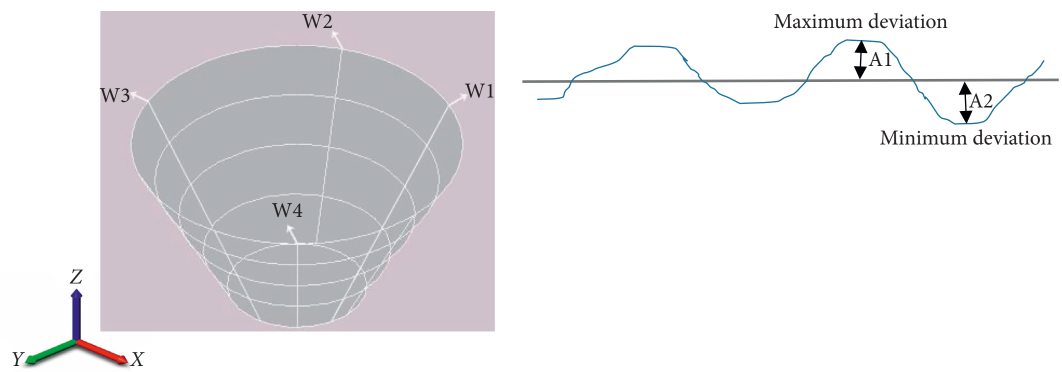

(a) (b)

Figure 3: (a) Surface waviness paths and (b) maximum and minimum deviation along path.

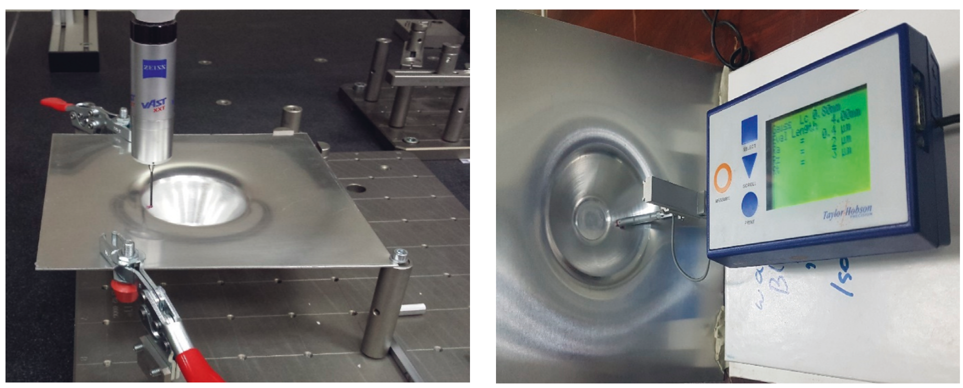

(a) (b)

Figure 4: Measurement setup: (a) CMM and (b) surface roughness.

The analysis of variance (ANOVA) was used to test the significant factors and interactions for each process output. The procedure used in this study was to run ANOVA with all terms (factors and interactions) included in the model. The model is then reduced by removing the terms that proved to be nonsignificant (with P values <0.05) one by one, unless it is a part of a significant higher level interaction [33–35]. The term with the greater P value is removed first and the fitting process is performed again. The ANOVA is rerun, and the elimination process is repeated until a reduced model with all significant terms is attained.

The model is further refined by removing readings with significant residuals from the reduced model [35, 36]. Hoaglin and Welsch [37] proposed that it is preferable to use standardized residuals (SR) in this regard. The SR is equal to the value of a residual divided by an estimate of its standard deviation. There is no specific limit for the SR to remove the readings; however, it was decided that only runs with $|SR| > 3.0$ would be removed from the model as they resemble a possible outlier.

The coefficient of determination values, R-squared, adjusted R-squared, and predicted R-squared, express the goodness of fit of the model, where R-squared is the general term used in models with a single factor, adjusted R-squared is preferred in models with multifactors, and predicted R-squared tests the overfitting of the model by estimating its ability to predict responses that are not included in the data. Values of coefficients of determination range between 0 and 1, where values close to 1 indicate better goodness of fit.

3.1. Analysis of Circularity Error. For better interpretation, the circularity error was normalized with respect to the part nominal diameter as the diameter is variable along the depth of the part. Therefore, the normalized circularity error (NC) (defined as the circularity error/the part nominal diameter) was the response considered in studying the factors affecting circularity error. Figure 5 shows the development of NC along the depth of the part, where NC1, NC2, and NC3 are the normalized circularity errors at the top, middle, and bottom of the part, respectively.

It can be clearly seen that the error increases as the tool goes down in the part. The NC values range approximately between 0.06 for NC1 and 0.1 for NC3.The illustrated trend as seen in Figure 5 is true for all cases. This could be explained by the fact that springback is the primary cause of profile errors in SPIF. As the tool moves down along the part depth, greater resistance to deformation is experienced, resulting in springback that leads to greater circularity error.

The ANOVA was only performed on NC3 as it had the greatest value of normalized circularity error as discussed in the previous paragraph. The ANOVA results indicate that

Table 2: DOE matrix and results.

Experiment no.	d	f	s	t	Waviness error (mm)				Circularity error (mm)			Roughness parameters (μm)		Side angle error (°)
					W1	W2	W3	W4	C1	C2	C3	Ra	Rt	
1	10	500	0.5	1	0.81	0.42	0.33	0.17	3.98	3.80	3.93	1.4	15.75	0.05
2	10	500	0.5	1	0.78	0.41	0.33	0.20	4.17	4.04	3.80	1.45	14.25	0.03
3	10	500	0.5	1	0.77	0.43	0.34	0.19	4.09	3.30	3.70	1.4	12.25	0.56
4	10	500	1	1	0.56	0.36	0.35	0.26	4.16	4.02	3.50	1.75	15.625	1.31
5	10	500	1	1	0.81	0.38	0.43	0.37	4.32	3.73	3.56	2.1	20.25	0.88
6	10	500	1	1	0.72	0.49	0.47	0.41	3.77	3.84	3.51	2.2	16.375	0.44
7	10	1000	0.5	1	0.37	0.18	0.34	0.48	3.62	3.74	3.60	2.3	19.875	0.03
8	10	1000	0.5	1	0.67	0.35	0.16	0.14	4.05	3.78	3.51	1.975	18.875	0.42
9	10	1000	0.5	1	0.53	0.22	0.25	0.16	3.56	3.56	3.60	1.475	16.75	0.27
10	10	1000	1	1	0.65	0.33	0.40	0.33	3.94	3.77	3.48	1.875	16.625	0.36
11	10	1000	1	1	0.88	0.39	0.65	0.43	3.77	3.55	3.34	2.025	15.875	0.09
12	10	1000	1	1	0.77	0.38	0.39	0.36	3.52	3.46	3.71	2.075	15.75	0.34
13	20	500	0.5	1	0.67	0.38	0.24	0.27	4.10	3.65	3.50	0.4	3.75	0.47
14	20	500	0.5	1	0.56	0.30	0.25	0.27	4.32	3.97	3.93	0.575	5.75	0.16
15	20	500	0.5	1	0.77	0.41	0.25	0.27	4.17	3.74	3.57	0.475	5.375	0.06
16	20	500	1	1	0.76	0.35	0.49	0.36	4.16	3.88	3.69	0.4	3.625	0.86
17	20	500	1	1	0.56	0.27	0.43	0.35	3.83	3.82	3.79	0.4	3.875	0.12
18	20	500	1	1	0.71	0.39	0.33	0.30	3.78	3.68	3.84	0.425	4.625	0.27
19	20	1000	0.5	1	0.68	0.40	0.26	0.27	4.21	3.36	3.50	0.425	5	0.41
20	20	1000	0.5	1	0.46	0.24	0.40	0.31	3.93	3.92	3.57	0.425	4.5	0.16
21	20	1000	0.5	1	0.59	0.28	0.42	0.30	4.22	3.45	3.65	0.425	4	0.03
22	20	1000	1	1	0.60	0.29	1.48	0.35	3.78	3.34	3.69	0.425	4.625	0.68
23	20	1000	1	1	0.74	0.40	0.28	0.25	3.87	3.91	3.85	0.4	4	0.11
24	20	1000	1	1	0.56	0.27	0.43	0.35	3.99	3.65	3.68	0.45	4.125	0.49
25	10	500	0.5	2	1.01	0.75	1.49	0.47	3.48	3.85	3.63	2.35	19.375	0.6
26	10	500	0.5	2	1.33	0.83	0.75	0.50	3.93	3.83	3.64	2.25	20.25	0.78
27	10	500	0.5	2	0.99	0.68	0.59	0.55	4.22	3.45	3.65	1.85	15.875	0.3
28	10	500	1	2	0.88	0.51	0.42	0.29	4.28	3.93	3.61	1.975	18.875	1.66
29	10	500	1	2	0.89	0.65	1.46	0.39	3.77	3.50	3.46	2.075	17.875	0.38
30	10	500	1	2	1.17	0.69	0.60	0.44	3.55	4.01	3.69	2.125	19.875	1.45
31	10	1000	0.5	2	1.20	0.80	1.46	0.49	4.12	3.84	4.05	2.5	18.625	0.4
32	10	1000	0.5	2	1.38	0.95	0.90	0.66	3.53	3.76	3.55	2.1	16.75	0.32
33	10	1000	0.5	2	1.27	0.75	0.70	0.44	4.21	3.48	3.56	1.825	13.875	0.49
34	10	1000	1	2	1.03	1.03	1.45	0.51	4.27	3.76	3.60	1.875	14.75	1.17
35	10	1000	1	2	1.16	0.85	0.76	0.56	3.75	4.11	3.59	2.3	19.375	1
36	10	1000	1	2	1.30	0.80	0.63	0.48	3.51	3.96	3.72	1.675	19.75	0.82
37	20	500	0.5	2	0.96	0.58	0.40	0.21	4.24	3.26	3.72	0.55	7.375	0.75
38	20	500	0.5	2	0.77	0.44	0.46	0.25	4.25	3.56	4.05	0.6	6.625	0.96
39	20	500	0.5	2	0.81	0.45	0.34	0.19	4.12	3.92	4.07	0.775	9.75	0.6
40	20	500	1	2	1.26	0.73	0.58	0.35	4.13	3.84	3.59	0.9	12.125	1
41	20	500	1	2	1.33	1.33	0.63	0.38	3.57	3.96	3.77	0.675	8.75	0.79
42	20	500	1	2	1.13	0.63	1.49	0.36	3.69	3.82	3.45	0.7	8.75	0.71
43	20	1000	0.5	2	0.84	0.48	0.49	0.27	4.11	3.79	3.82	0.525	5.625	0.93
44	20	1000	0.5	2	0.95	0.55	0.67	0.27	4.04	3.92	3.76	0.55	5.25	0.61
45	20	1000	0.5	2	1.00	0.54	0.54	0.26	4.08	3.72	3.85	0.475	4.125	1.05
46	20	1000	1	2	1.20	0.71	1.42	0.43	3.56	3.91	3.57	0.7	11.125	1.13
47	20	1000	1	2	1.19	0.68	0.68	0.44	4.18	3.86	3.61	0.65	8.5	1.07
48	20	1000	1	2	1.27	0.74	0.69	0.44	4.05	3.81	3.60	0.525	5.125	1.14

the three-way interaction between d, s, and t had the most significant effect on the circularity error. To reduce the error, the appropriate proportions between the levels of the three interaction factors must be selected.

Figure 6 shows the three-way interaction between d, s, and t where the two-way interaction $d * s$ is presented at two different levels of t (1.0 and 2.0 mm.) The differences in $d * s$ interaction pattern with the change in t value proves the significant three-way interaction. Within the studied range and for thin sheets, low circularity error can be achieved using small d and large s or small s and large d. The worst circularity error occurs when using both large d and s. For thick sheets, using big d, circularity error does not change with s, while the worst circularity error occurs at small d and large s.

The value of adjusted R-squared shows that the model can explain 53% of the variations in the data, and it can be

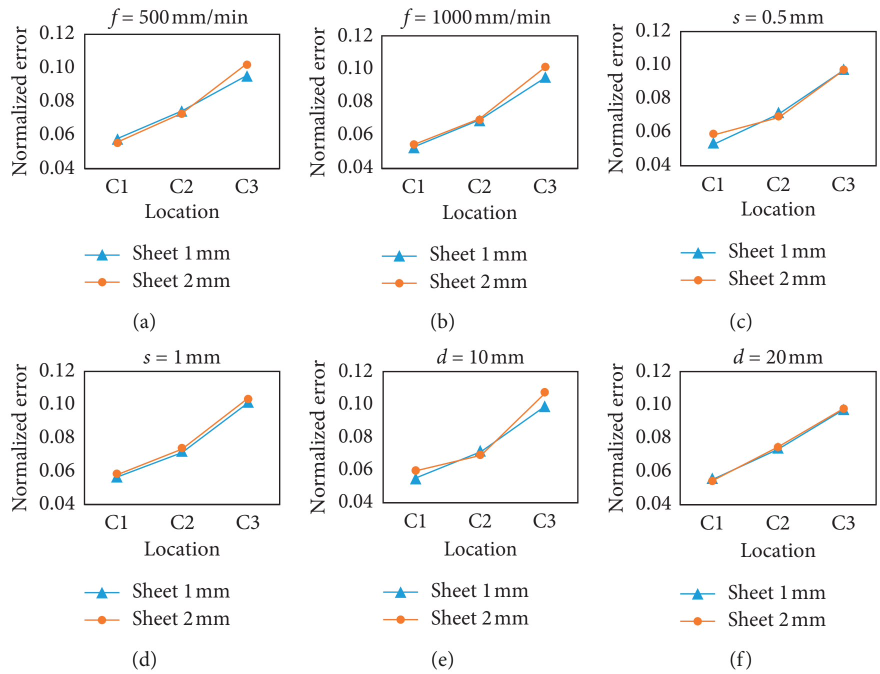

Figure 5: (a) and (b) Effect of f on normalized circularity error at $d = 20$ mm and $s = 0.5$ mm, (c) and (d) effect of s on normalized circularity error at $d = 10$ mm and $f = 1000$ mm, and (e) and (f) effect of d on normalized circularity error at $f = 500$ mm and $s = 1$ mm.

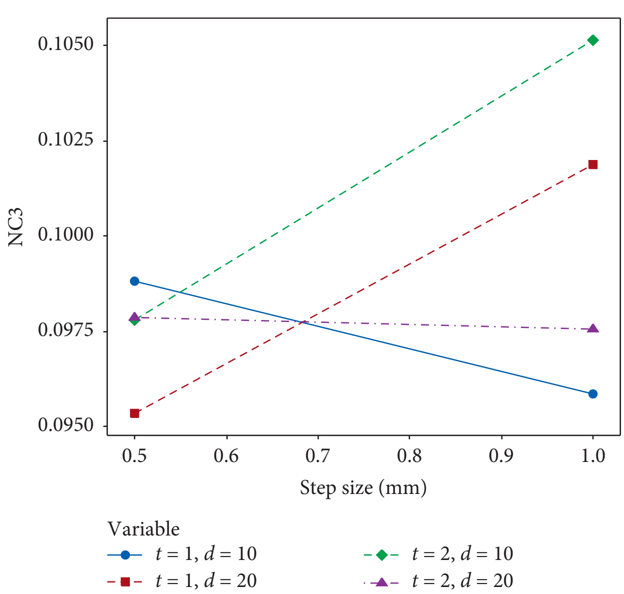

Figure 6: Three-way interaction plot for normalized circularity error.

seen that 47% of the variations originate from unknown nuisance factors. ANOVA results imply that the levels of d and s, in relation to t, could be selected in such a way that favors the ISF limit. For example, smaller values of s and d would be recommended [2] for thick sheets. While this combination is not advised for thin sheets, a compromise could be made depending on the situation. However, as mentioned before, the circularity error depends more on the location within the formed part rather than explicitly on individual parameters, allowing more flexibility for the part designer (Table 3 and Figure 5).

Table 3: ANOVA results for normalized circularity error (NC3).

Source	DF	Adj SS	Adj MS	F value	P value
Regression	7	0.000421	0.00006	7.93	<0.01
d	1	0.00002	0.00002	2.59	0.116
s	1	0.00008	0.00008	10.57	0.002
t	1	0.000021	0.000021	2.78	0.104
$d*s$	1	0.000001	0.000001	0.09	0.761
$d*t$	1	0.000068	0.000068	9.00	0.005
$s*t$	1	0.000002	0.000002	0.33	0.57
$d*s*t$	1	0.000197	0.000197	25.96	0.01
Error	36	0.000273	0.000008		
Lack-of-Fit	8	0.000061	0.000008	1.01	0.454
Pure error	28	0.000212	0.000008		
Total	43	0.000694			
Model summary	R-sq 53.01%	R-sq (adj) 60.66%		R-sq (pred) 42.43%	

3.2. Analysis of Waviness Error. Figure 7 shows the development of the waviness error along 30 mm of the part depth in four randomly selected parts. It can be seen in the figure that the waviness error changes value and direction along the part depth. The maximum waviness error (about 0.2 mm) is noticed at the middle of the part where the part wall support is the minimum. As the part wall is supported at the top by the fixture and at the bottom by the part base, less waviness error takes place. It is expected that, as the part designed depth increases, the side wall waviness error will also increase.

It is also noted in Table 2 that the values of waviness errors at the four locations, W1, W2, W3, and W4, are different. This might be attributed to using the transition

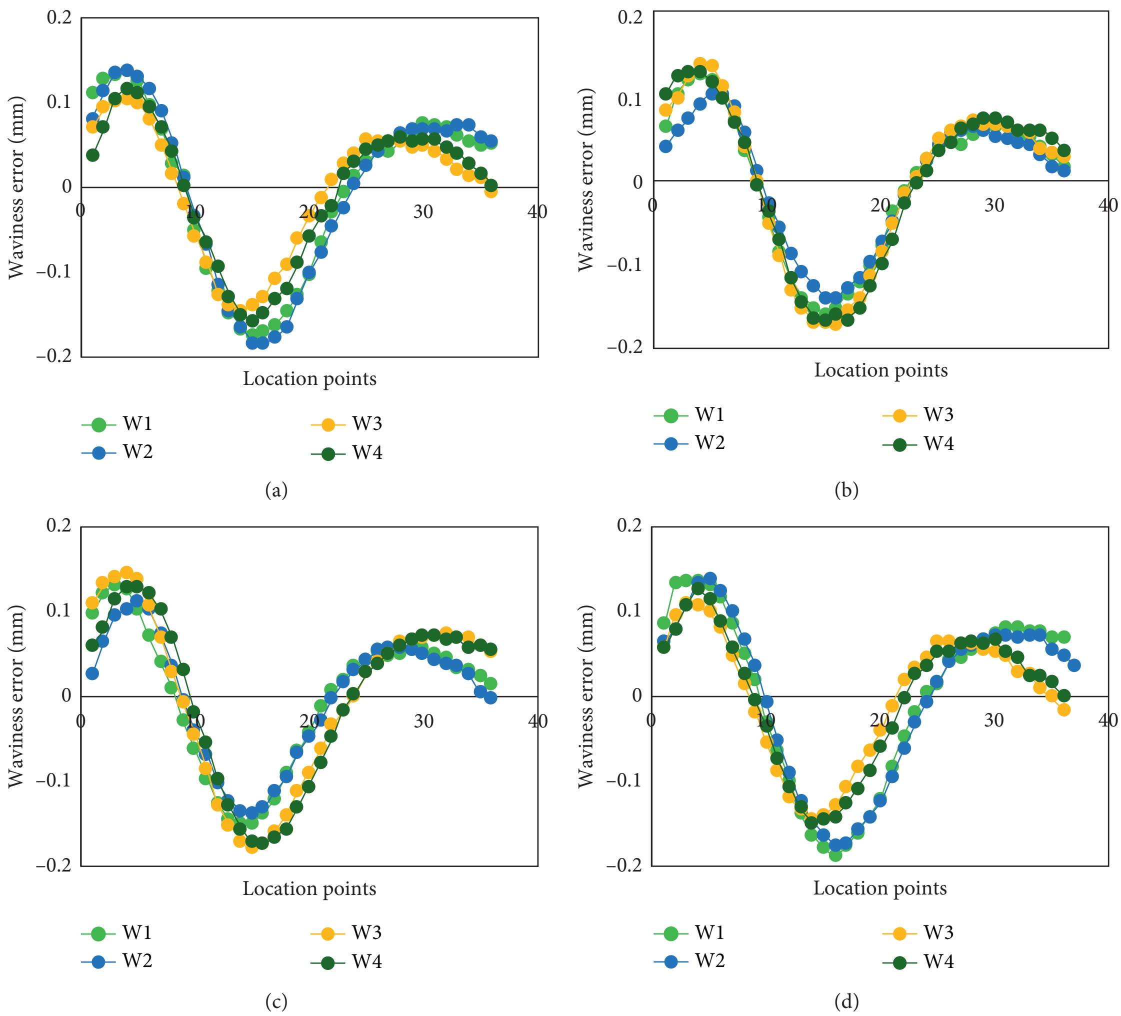

FIGURE 7: Randomly selected parts: (a) experiment no. 10, (b) experiment no. 38, (c) experiment no. 12, and (d) experiment no. 9.

step method where the tool completes 360° on the sheet and then steps down in the Z-direction by the selected step value. A seam line can be detected along the part depth at the step position as shown in Figure 8. This seam line and the surrounding area on the formed part represent highly plastically deformed region. This leads to differences amongst the waviness error values depending on their distance from the seam line. The waviness errors measured near the seam lines are usually higher than those measured far from the seam line.

The ANOVA results for waviness error, presented in Table 4, indicate that the most significant terms are the two-way interactions $d * s$ and $d * t$. The model adequacy evaluation is presented in Table 4. The value of adjusted R-squared indicates that the model explains 74.6% of the variations in the data.

Approximately 25% of the variation comes from unknown nuisance factors.

Figure 9 shows the interaction plots of $d * s$ and $d * t$ that indicate that with a greater d, a smaller s clearly improves the part waviness, while smaller d exhibits no clear difference. Therefore, as in the case of circularity errors, the thin sheet exhibited better surface waviness compared to the thick sheet. Moreover, it can be seen that the effect of tool diameter on waviness error is not significant for thin sheets, while for thick sheets, big tool diameter reduces the waviness error. However, the tool diameter should be increased keeping in view the restrictions imposed regarding the formability limit. That is ISF limit decreases as the tool diameter increases [1, 2].

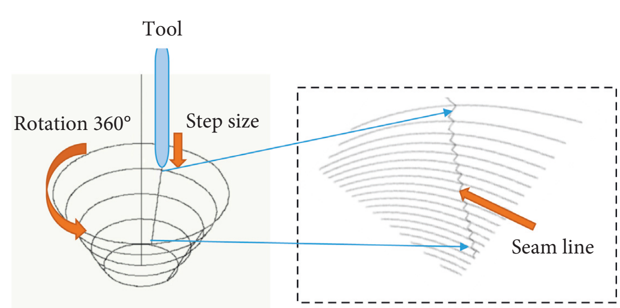

FIGURE 8: Transition step method.

Table 4: ANOVA results for waviness error.

Source	DF	Adj SS	Adj MS	F value	P value
Regression	5	2.95	0.59	28.64	<0.01
d	1	0.02	0.02	0.94	0.337
s	1	0.06	0.06	3.09	0.086
t	1	0.64	0.64	31.10	<0.01
$d * s$	1	0.18	0.18	8.80	0.005
$d * t$	1	0.11	0.11	5.53	0.023
Error	42	0.86	0.02		
Lack-of-Fit	10	0.40	0.04	2.71	0.016
Pure error	32	0.46	0.015		
Total	47	3.81			
Model summary	R-sq 77.32%		R-sq (adj) 74.62%		R-sq (pred) 70.38%

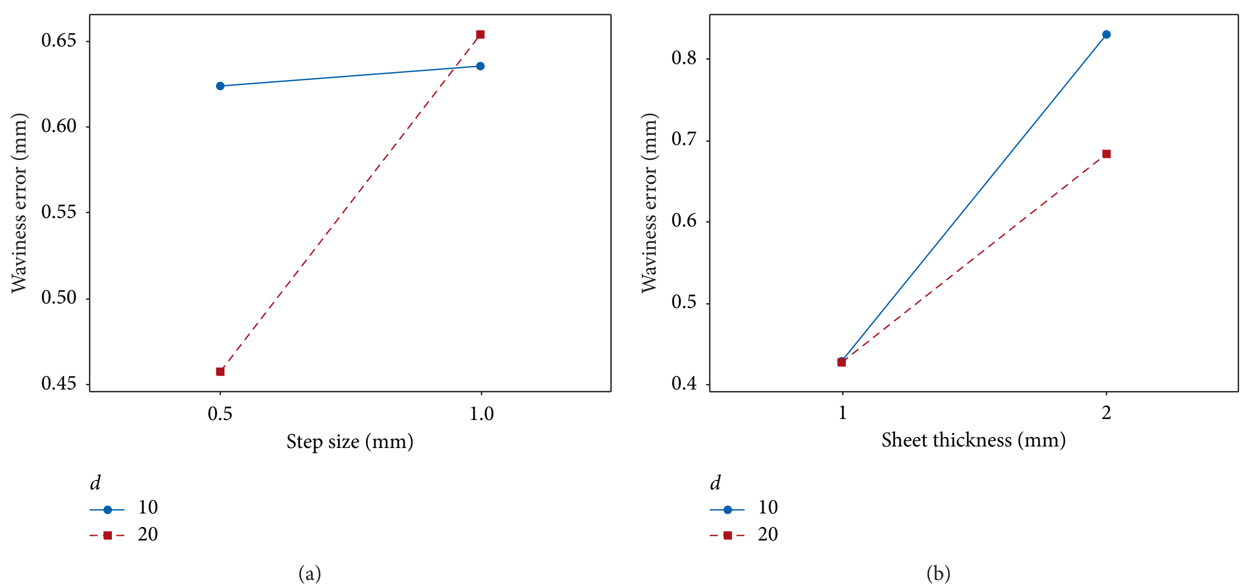

Figure 9: Interaction plot for waviness error.

Table 5: ANOVA results for side angle error.

Source	DF	Adj SS	Adj MS	F	P value
Main effects	2	9.67	4.83	65.82	<0.01
s	1	2.88	2.88	39.23	<0.01
t	1	6.59	6.59	89.76	<0.01
Residual error	42	3.09	0.07		
Pure error	41	3.01	0.07		
Total	44				
Model summary	R-sq 75.81%		R-sq (adj) 74.66%		R-sq (pred) 72.22%

3.3. Analysis of Side Angle Error. Table 5 presents the ANOVA results for side angle errors. The results indicate that only the factors s and t have significant effects on the error. The value of adjusted R-squared shows that the model explains 74.7% of the variation in the data. Approximately 25% of the variation comes from unknown nuisance factors.

Figure 10 shows the main effect plots for the two significant factors. The results indicate that thin sheets and small steps reduce the error in the side wall angle. The minimum error is almost doubled as s changes from 0.5 to 1.0 mm and tripled as the thickness changes from 1 to 2 mm. This is due to the reason that, as the sheet thickness increases, the sheet becomes more rigid, and as the step size increases, more plastic deformation happens in the formed part due to which the side angle error increases. Reducing the step size to minimize the side wall angle error will also enhance the ISF limit.

3.4. Analysis of Surface Roughness. It can be seen in Figure 11 that d has the most significant effect on surface roughness and that the roughness (both Ra and Rt) is decreased by up to four times by increasing the diameter of the forming tool from 10 mm to 20 mm. The poor surface finish generated with the smaller d forming tool could be because of its

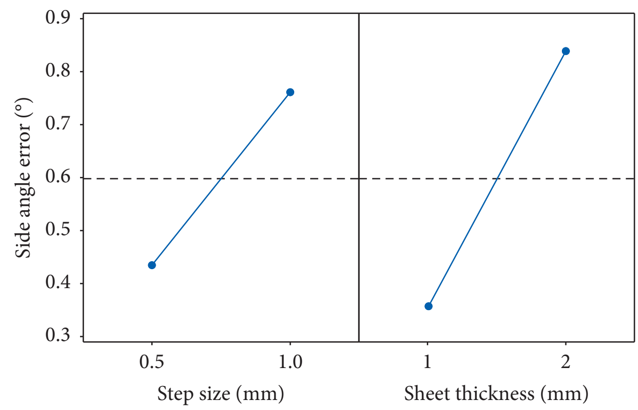

Figure 10: Main effects of side angle error.

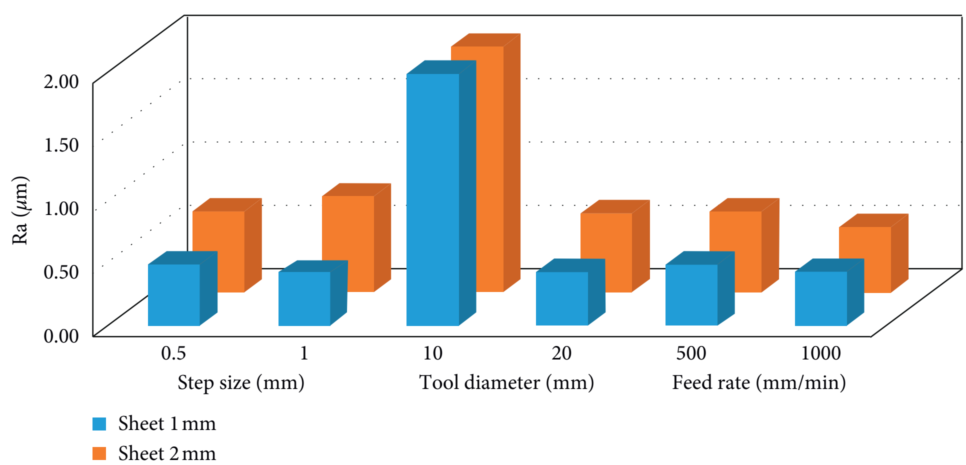

(a)

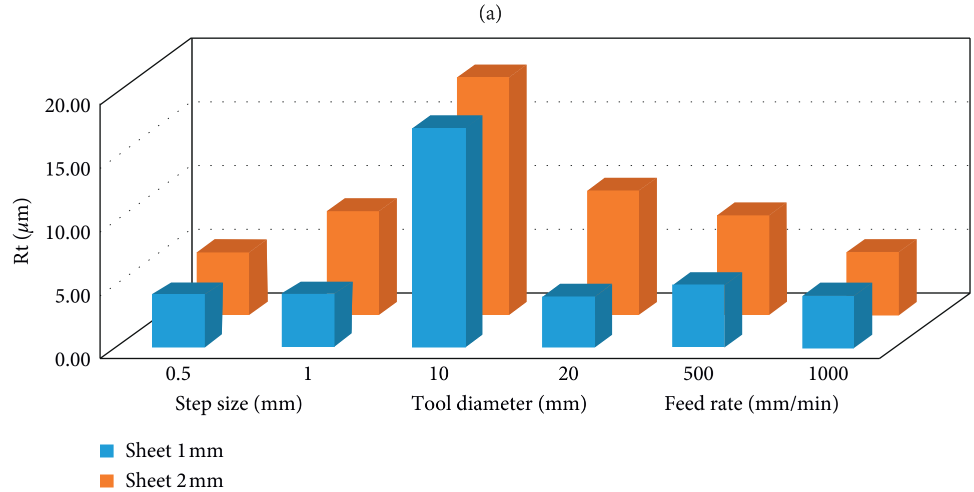

(b)

Figure 11: Influence of s, d, f, and t on surface roughness Ra and Rt.

excessive wear during the forming process as compared to the tool with the greater d. This difference in the wear at the contacting tip of the two tools can be seen in Figure 12.

The greater wear in the smaller tool is caused by contact forces acting on a smaller area resulting in higher stresses when compared to larger tools. It can be seen in Figure 13 that the forming forces applied on the small tool are higher than that of the bigger tool even when all the other process parameters are constant [38, 39]. Also Figure 14 shows that the initial roughness of the two SPIF tools is almost the same. Since the two tools have the same starting roughness during the SPIF process, they undergo different forming forces; therefore, they show different tool wears which is due to the difference between their diameters. The two tools show

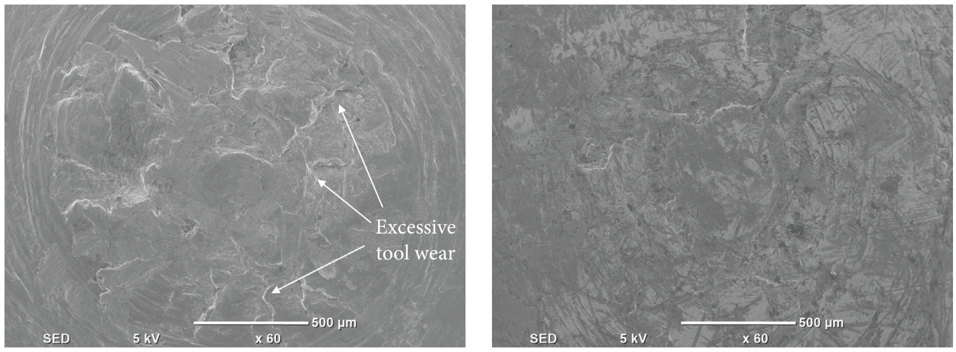

(a) (b)

Figure 12: Scanning electron microscope images of contacting tip of tool: (a) smaller tool $d = 10$ mm and (b) larger tool $d = 20$ mm.

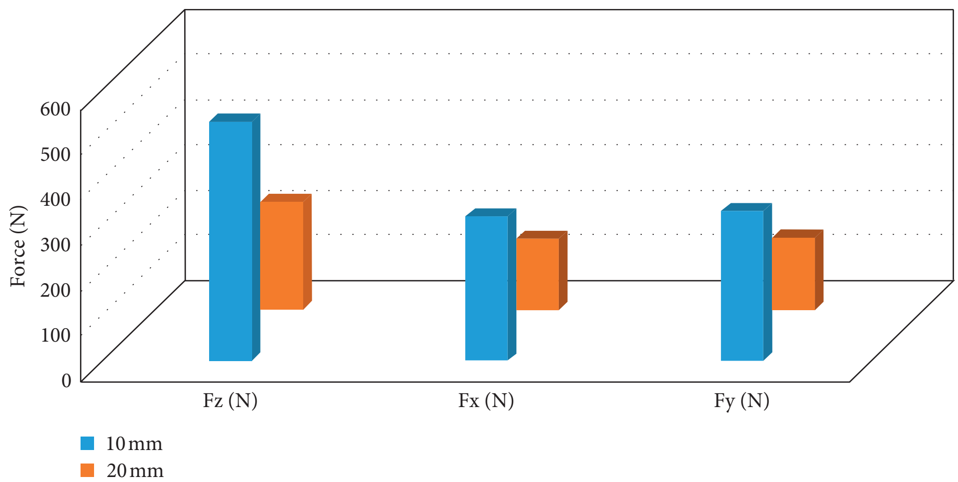

Figure 13: Forming force with different tool diameter at $f = 500$ mm/min, $s = 1$ mm, and $t = 1$ mm.

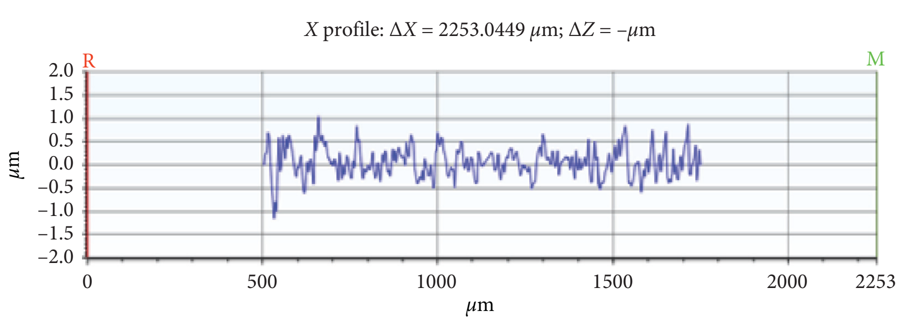

Label	Value	Units
Ra	0.329	μm
Rp	1.334	μm
Rq	0.415	μm
Rz	1.729	μm

(a)

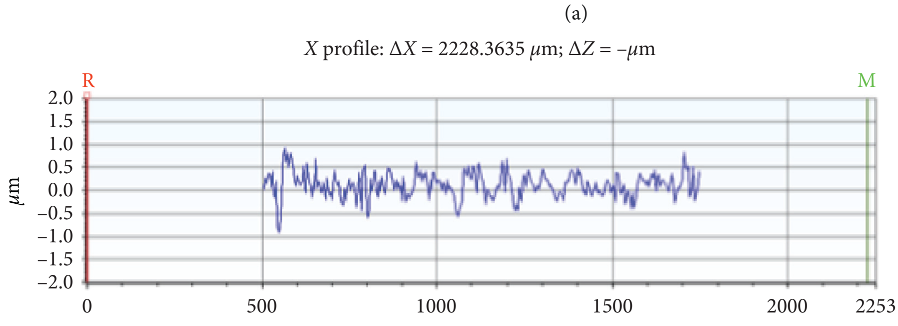

Label	Value	Units
Ra	0.308	μm
Rp	1.328	μm
Rq	0.412	μm
Rz	1.871	μm

(b)

Figure 14: Initial surface roughness of tools: (a) 10 mm tool diameter; (b) 20 mm tool diameter.

Table 6: ANOVA results for surface roughness (Ra).

Source	DF	Adj SS	Adj MS	F value	P value
Model	2	24.77	12.38	270.68	0.00
Linear	2.00	24.77	12.38	270.68	0.00
d	1.00	24.19	24.19	528.69	0.01
t	1.00	0.58	0.58	12.67	0.01
Lack-of-Fit	13.00	0.90	0.07	1.90	0.07
Pure error	32.00	1.16	0.04		
Total	47.00	26.83			
Model summary	R-sq 92.33%	R-sq (adj) 91.98		R-sq (pred) 91.27%	

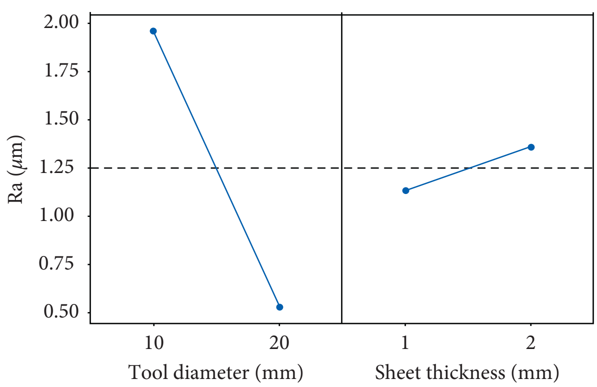

Figure 15: Main effects of surface roughness Ra.

different wear rates as shown in Figure 12; the rate is higher in the tool with smaller diameter and less in the tool with the larger diameter. Therefore, the resulting surface on the formed part will also show the difference in the roughness from the two tools, and this difference is due to the difference in the tools diameters only.

The surface roughness is also affected by t with any combination of the other input parameters. In addition, it appears as if the roughness is not influenced by s or f. In order to improve the roughness, larger tool diameter should be accompanied with smaller value of s and bigger value of f in order not to adversely affect the ISF limit [2].

Table 6 presents the ANOVA results for Ra. The results indicate that only the factors d and t have a significant effect on Ra. The value of adjusted R-squared indicates that the model explains 92% of the variations in the data. Approximately 8% of the variation comes from unknown nuisance factors. Figure 15 shows the main effects plots for the two significant factors.

4. Conclusions

This study presented the significance of controlling the process parameters in order to enhance the surface roughness and the surface profile accuracy in terms of reducing the circularity, waviness, and side wall angle errors. For the first time, the effects of the SPIF process parameters were considered on the circularity and waviness errors of the formed parts. The influential process parameters and their contribution to the profile accuracy and surface roughness are summarized as follows:

(i) Regarding the circularity error, it is concluded that it mainly depends on the location within the formed part. Circularity error significantly increases along the depth of the part. Furthermore, the error is also affected by the triple interaction between d, s, and t.

(ii) Considering the waviness error, it is concluded that the error change in a sinusoidal pattern along the depth of the part. This error was dominated primarily by t and the interaction of d with t and s. For thin sheets, the tool diameter does not have a significant effect on the waviness error. However, as the sheet thickness increases, bigger tool diameter is needed to keep the error low.

(iii) With respect to the side angle error, the significant factors are t and s. The error increases with the increase in both t and s due to the increase in the springback effect.

(iv) Regarding the surface roughness, the dominating factor is d. This is because more tool wear occurred on the smaller tools, using the same process parameters, which leads to the degraded surface roughness.

In summary, smaller t, bigger d, and smaller s yield improved profile accuracy and surface quality in terms of reducing waviness, circularity, and side angle errors. Regarding the waviness error, the thin sheet exhibits higher local springback that leads to reducing the deviation between the peaks and valleys of the measured surface. This is because the thin sheet is more elastic or more flexible geometrically; therefore, when the tool exerts forces on it, the plastic deformation is less and there is more elastic deformation due to its flexibility. However, as the same forces are exerted on the thick sheet, which actually is more rigid as compared to the thin sheet, the forces being exerted on it will be creating more plastic deformations that is higher deviation between the peaks and valleys of the measured surface. Same phenomenon is applicable to the circularity error, that is for less sheet thickness the circularity error will be less and vice versa.

However, smaller t and bigger d could reduce the formability limit. Care must be taken in selecting the process parameters values in case of producing parts that approaches the fracture limit.

Data Availability

The experimental data used to support the findings of this study are included within the article.

Conflicts of Interest

The authors declare that they have no conflicts of interest.

Acknowledgments

The authors extend their appreciation to the Deanship of Scientific Research at King Saud University for funding this work through research group no. (RG-1439-005). The authors thank the Deanship of Scientific Research and RSSU at King Saud University for their technical support.

References

[1] G. Ambrogio and L. Filice, "On the use of Back-drawing Incremental Forming (BIF) to improve geometrical accuracy in sheet metal parts," *International Journal of Material Forming*, vol. 5, no. 4, pp. 269–274, 2012.

[2] J. Jeswiet, F. Micari, G. Hirt, A. Bramley, J. Duflou, and J. Allwood, "Asymmetric single point incremental forming of sheet metal," *CIRP Annals*, vol. 54, no. 2, pp. 88–114, 2005.

[3] G. Ambrogio, L. De Napoli, L. Filice, F. Gagliardi, and M. Muzzupappa, "Application of Incremental Forming process for high customised medical product manufacturing," *Journal of Materials Processing Technology*, vol. 162-163, pp. 156–162, 2005.

[4] V. Oleksik, A. Pascu, C. Deac, R. Fleaca, M. Roman, and O. Bologa, "The influence of geometrical parameters on the incremental forming process for knee implants analyzed by numerical simulation," in *Proceedings of the NUMIFORM*, pp. 1208–1215, Pohang, Republic of Korea, June 2010.

[5] A. Attanasio, E. Ceretti, C. Giardini, and L. Mazzoni, "Asymmetric two points incremental forming: improving surface quality and geometric accuracy by tool path optimization," *Journal of Materials Processing Technology*, vol. 197, no. 1–3, pp. 59–67, 2008.

[6] H. Iseki and H. Kumon, "Forming limit of incremental sheet metal stretch forming using spherical rollers," *Journal-Japan Society for Technology of Plasticity*, vol. 35, no. 11, p. 1336, 1994.

[7] H. Iseki, K. Kato, and S. Sakamoto, "Flexible and incremental sheet metal forming using a spherical roller," in *Proceedings of the 40th JJCTP*, pp. 41–44, 1989, in Japanese.

[8] G. Ambrogio, I. Costantino, L. De Napoli, L. Filice, L. Fratini, and M. Muzzupappa, "Influence of some relevant process parameters on the dimensional accuracy in incremental forming: a numerical and experimental investigation," *Journal of Materials Processing Technology*, vol. 153-154, pp. 501–507, 2004.

[9] E. Hagan and J. Jeswiet, "A review of conventional and modern single-point sheet metal forming methods," *Proceedings of the Institution of Mechanical Engineers, Part B: Journal of Engineering Manufacture*, vol. 217, no. 2, pp. 213–225, 2003.

[10] M. Bambach, B. Taleb Araghi, and G. Hirt, "Strategies to improve the geometric accuracy in asymmetric single point incremental forming," *Production Engineering*, vol. 3, no. 2, pp. 145–156, 2009.

[11] H. Iseki and T. Naganawa, "Vertical wall surface forming of rectangular shell using multistage incremental forming with spherical and cylindrical rollers," *Journal of Materials Processing Technology*, vol. 130-131, pp. 675–679, 2002.

[12] G. Hirt, M. Bambach, S. Junk, and I. Chouvalova, "FEM modelling and optimisation of geometric accuracy in incremental CNC sheet forming," in *Proceeding of the Tenth Saxon Conference on Forming Technology*, Chemnitz, Germany, 2003.

[13] G. Hussain, G. Lin, and N. Hayat, "Improving profile accuracy in SPIF process through statistical optimization of forming parameters," *Journal of Mechanical Science and Technology*, vol. 25, no. 1, pp. 177–182, 2011.

[14] G. Ambrogio, V. Cozza, L. Filice, and F. Micari, "An analytical model for improving precision in single point incremental forming," *Journal of Materials Processing Technology*, vol. 191, no. 1-3, pp. 92–95, 2007.

[15] G. Hussain and L. Gao, "A novel method to test the thinning limits of sheet metals in negative incremental forming," *International Journal of Machine Tools and Manufacture*, vol. 47, no. 3-4, pp. 419–435, 2007.

[16] A. Petek, K. Kuzman, and J. Kopač, "Deformations and forces analysis of single point incremental sheet metal forming," *International Scientific Journal of Archives of Materials Science and Engineering*, vol. 35, no. 2, pp. 107–116, 2009.

[17] E. Hagan and J. Jeswiet, "Analysis of surface roughness for parts formed by computer numerical controlled incremental forming," *Proceedings of the Institution of Mechanical Engineers, Part B: Journal of Engineering Manufacture*, vol. 218, no. 10, pp. 1307–1312, 2004.

[18] G. Hussain, L. Gao, N. Hayat, Z. Cui, Y. C. Pang, and N. U. Dar, "Tool and lubrication for negative incremental forming of a commercially pure titanium sheet," *Journal of Materials Processing Technology*, vol. 203, no. 1–3, pp. 193–201, 2008.

[19] M. Durante, A. Formisano, and A. Langella, "Comparison between analytical and experimental roughness values of components created by incremental forming," *Journal of Materials Processing Technology*, vol. 210, no. 14, pp. 1934–1941, 2010.

[20] Z. Liu, S. Liu, Y. Li, and P. A. Meehan, "Modeling and optimization of surface roughness in incremental sheet forming using a multi-objective function," *Materials and Manufacturing Processes*, vol. 29, no. 7, pp. 808–818, 2014.

[21] I. Bagudanch, M. L. Garcia-Romeu, G. Centeno, A. Elías-Zúñiga, and J. Ciurana, "Forming force and temperature effects on single point incremental forming of polyvinylchloride," *Journal of Materials Processing Technology*, vol. 219, pp. 221–229, 2015.

[22] V. Mugendiran, A. Gnanavelbabu, and R. Ramadoss, "Parameter optimization for surface roughness and wall thickness on AA5052 Aluminium alloy by incremental forming using response surface methodology," *Procedia Engineering*, vol. 97, pp. 1991–2000, 2014.

[23] A. Bhattacharya, K. Maneesh, N. V. Reddy, and J. Cao, "Formability and surface finish studies in single point incremental forming," *Journal of Manufacturing Science and Engineering*, vol. 133, no. 6, Article ID 061020, 2011.

[24] B. Lu, J. Chen, H. Ou, and J. Cao, "Feature-based tool path generation approach for incremental sheet forming process," *Journal of Materials Processing Technology*, vol. 213, no. 7, pp. 1221–1233, 2013.

[25] Y. H. Kim and J. J. Park, "Effect of process parameters on formability in incremental forming of sheet metal," *Journal of Materials Processing Technology*, vol. 130-131, pp. 42–46, 2002.

[26] B. Lu, Y. Fang, D. K. Xu et al., "Mechanism investigation of friction-related effects in single point incremental forming using a developed oblique roller-ball tool," *International Journal of Machine Tools and Manufacture*, vol. 85, pp. 14–29, 2014.

[27] G. Hussain, L. Gao, N. Hayat, and X. Ziran, "A new formability indicator in single point incremental forming," *Journal of Materials Processing Technology*, vol. 209, no. 9, pp. 4237–4242, 2009.

[28] R. Malhotra, L. Xue, T. Belytschko, and J. Cao, "Mechanics of fracture in single point incremental forming," *Journal of Materials Processing Technology*, vol. 212, no. 7, pp. 1573–1590, 2012.

[29] M. B. Silva, P. S. Nielsen, N. Bay, and P. A. Martins, "Failure mechanisms in single-point incremental forming of metals," *The International Journal of Advanced Manufacturing Technology*, vol. 56, no. 9-12, pp. 893–903, 2011.

[30] A. Fiorentino, "Force-based failure criterion in incremental sheet forming," *The International Journal of Advanced Manufacturing Technology*, vol. 68, no. 1–4, pp. 557–563, 2013.

[31] V. A. Cristino, L. Montanari, M. B. Silva, A. G. Atkins, and P. A. F. Martins, "Fracture in hole-flanging produced by single point incremental forming," *International Journal of Mechanical Sciences*, vol. 83, pp. 146–154, 2014.

[32] ISO 230-4, *Test Code for Machine Tools—Part 4: Circular Tests for Numerically Controlled Machine Tools*, ISO, Geneva, Switzerland, 2005.

[33] Y. Zhang and K. Chou, "A parametric study of part distortions in fused deposition modelling using three-dimensional finite element analysis," *Proceedings of the Institution of Mechanical Engineers, Part B: Journal of Engineering Manufacture*, vol. 222, no. 8, pp. 959–968, 2008.

[34] D. Fydrych and G. Rogalski, "Effect of shielded-electrode wet welding conditions on diffusion hydrogen content in deposited metal," *Welding International*, vol. 25, no. 3, pp. 166–171, 2011.

[35] T. Ding, S. Zhang, Y. Wang, and X. Zhu, "Empirical models and optimal cutting parameters for cutting forces and surface roughness in hard milling of AISI H13 steel," *The International Journal of Advanced Manufacturing Technology*, vol. 51, no. 1–4, pp. 45–55, 2010.

[36] T. C. Patel, L. S. Patel, and B. C. Patel, "Analysis and prediction of milling process on vertical milling centre (VMC) by using response surface methodology (RSM)," *International Journal for Innovative Research in Science and Technology*, vol. 1, no. 7, pp. 205–212, 2015.

[37] D. C. Hoaglin and R. E. Welsch, "The hat matrix in regression and ANOVA," *The American Statistician*, vol. 32, no. 1, pp. 17–22, 1978.

[38] A. Dabwan, A. E. Ragab, M. A. E. Saleh, and A. K. Daoud, "Determining the effect of key process parameters on forming force of single point incremental sheet metal forming," in *Proceedings of the International Conference on Industrial Engineering and Operations Management*, Kuala Lumpur, Malaysia, March 2016.

[39] A. Alsamhan, A. E. Ragab, A. Dabwan, M. M. Nasr, and L. Hidri, "Prediction of formation force during single-point incremental sheet metal forming using artificial intelligence techniques," *PLoS One*, vol. 14, no. 8, Article ID e0221341, 2019.

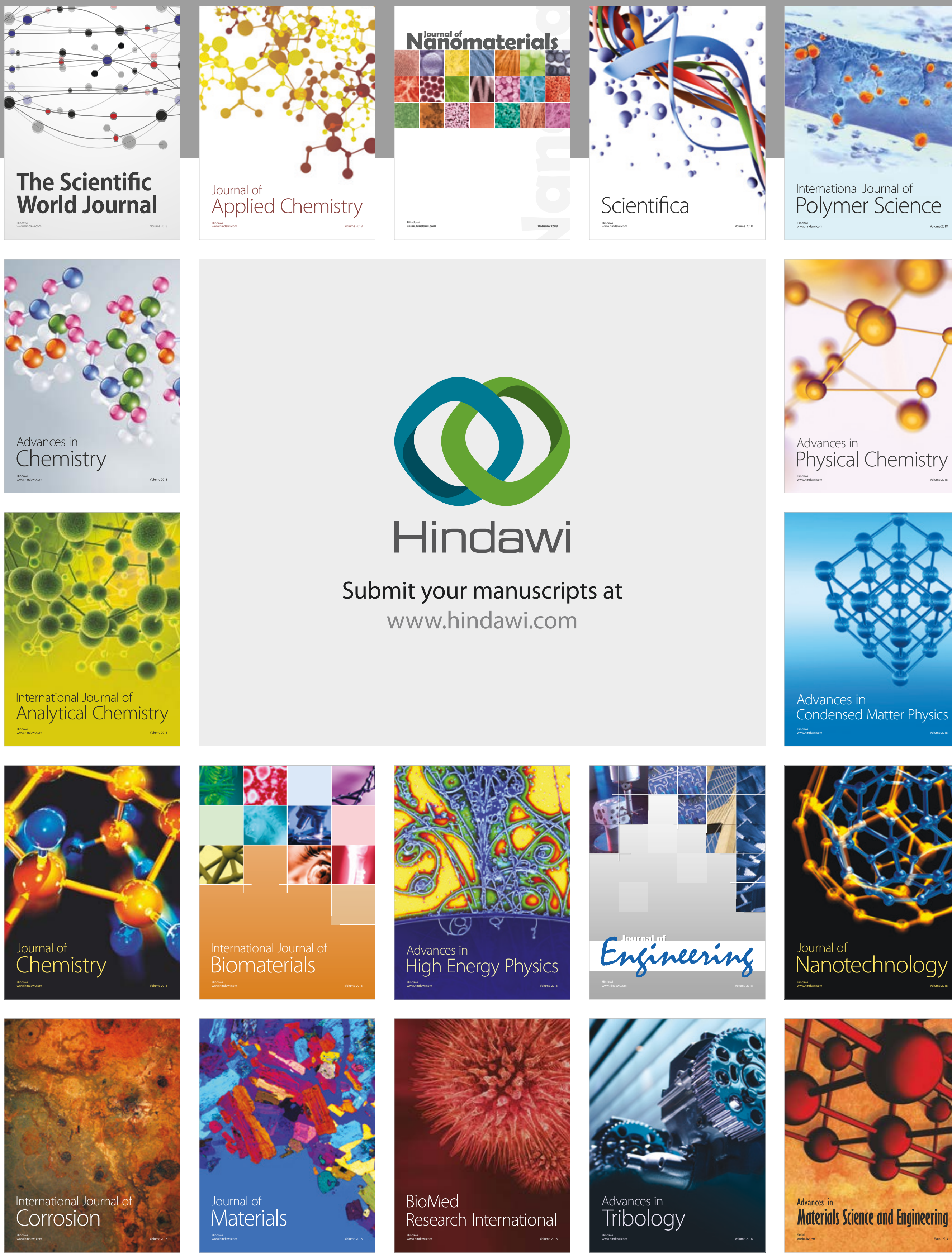
The Scientific World Journal
Journal of Applied Chemistry
Journal of Nanomaterials
Scientifica
International Journal of Polymer Science
Advances in Chemistry
Hindawi
Submit your manuscripts at
www.hindawi.com
Advances in Physical Chemistry
International Journal of Analytical Chemistry
Advances in Condensed Matter Physics
Journal of Chemistry
International Journal of Biomaterials
Advances in High Energy Physics
Journal of Engineering
Journal of Nanotechnology
International Journal of Corrosion
Journal of Materials
BioMed Research International
Advances in Tribology
Advances in Materials Science and Engineering